Organic & Biomolecular Chemistry

PAPER

View Article Online
View Journal | View Issue

Cite this: *Org. Biomol. Chem.*, 2018, **16**, 8613

Porphyrin–ferrocene conjugates for photodynamic and chemodynamic therapy†

Zhitao Lei,[a,b] Xiaoyu Zhang,*[a] Xiaohua Zheng,[b,c] Shi Liu[b] and Zhigang Xie *[b]

Received 26th September 2018,
Accepted 25th October 2018

DOI: 10.1039/c8ob02391c

rsc.li/obc

Chemodynamic therapy can convert endogenous hydrogen peroxide (H_2O_2) at tumor localization into the toxic hydroxyl radical (˙OH) destroying tumor cells. Photodynamic therapy as a noninvasive method utilizes photosensitizers (PSs) to convert O_2 into cytotoxic reactive oxygen species (*e.g.*, $^1O_2$) upon laser irradiation, which is dependent on the content of oxygen. The combination of the two therapeutic strategies on a single platform can enhance the anticancer effect. Herein, we report a porphyrin–ferrocene theranostic agent for combined photodynamic and chemodynamic therapy. Compared to monotherapy, the as-prepared porphyrin–ferrocene conjugates exhibit superior efficiency and potency in killing cancer cells at low drug doses. This study suggests the rational design of molecular structures as multifunctional therapeutics for potential clinic application.

Introduction

Despite the rapid advances in medical technology, cancer is still a difficult problem to be overcome. The high mortality rate of cancer has led to the rapid development of various treatments, including surgery, chemotherapy, radiotherapy and phototherapy.[1–5] Reactive oxygen species (ROS), including the superoxide anion, hydrogen peroxide (H_2O_2), singlet oxygen and hydroxyl radicals, possess the ability to efficiently kill cancer cells.[6,7] In recent years, a lot of effort has been invested on the development strategy of cancer treatment through ROS, such as chemodynamic therapy and photodynamic therapy. Chemodynamic therapy (CDT) produces ROS using endogenous chemical energy, which could evoke cell death, in the absence of additional energy stimulation (*e.g.*, laser irradiation).[8–16] Fenton or Fenton-like reactions can not only generate the most toxic ROS (˙OH) by disproportionation reactions of H_2O_2 but also produce O_2 in excess of H_2O_2. Fenton-like reactions are commonly used in CDT, for example, ferrocene (FC) and its derivatives can generate hydroxyl radicals (˙OH, the most poisonous ROS) in the presence of hydrogen peroxide (H_2O_2).[17–21] In addition, Lin and co-workers developed a manganese dioxide (MnO_2)-based nanoagent as a CDT agent, which possesses both glutathione (GSH) diminution properties and Fenton-like Mn^{2+} delivery.[10] However, the treatment effect of CDT is greatly weakened because of the reaction of between ˙OH and GSH in cancer cells.

As a noninvasive cancer treatment, phototherapy mainly includes photothermal and photodynamic therapy (PDT).[22–31] Photosensitizers can transfer energy from light to the surrounding molecular oxygen and produce poisonous ROS, especially singlet oxygen ($^1O_2$), which can lead to increased permeability of the cell membranes and further interfering with the normal function of cells. Porphyrin and its derivatives have been proposed as potential photosensitizers for PTT[32–35] and PDT, owing to their high photostability and good biocompatibility.[4,36–41] However, because of tissue hypoxia and limited light penetration, the photodynamic effects of porphyrin alone exhibit insufficiency of treatment to some extent. Therefore, it is important and imperative to combine PDT with other treatment methods, such as chemotherapy and CDT.[11,42–46] Chemodynamic therapy (CDT) can convert endogenous hydrogen peroxide (H_2O_2) at tumor localization into the toxic hydroxyl radical (˙OH) destroying tumor cells, thus making up for the O_2-dependent limitations of PDT to a degree. Synergistic effects of PDT and CDT could enhance the treatment efficiency of malignant tumors. The combination of chemotherapy and PDT has been expanded and proved to be an efficient approach to gain an optimal treatment outcome and reduce the side effects of each treatment method.

Herein, we synthesized an agent porphyrin–ferrocene (TNCF) from porphyrin and ferrocene, which combines CDT with PDT (Scheme 1A). Although there are some reports about porphyrin–ferrocene conjugates,[47,48] their application in

[a]*College of Environmental and Chemical Engineering, Yanshan University, 438 Heibei Avenue, Qinhuangdao, Hebei 066004, P. R. China. E-mail: xiaoyuzhang@ysu.edu.cn*
[b]*State Key Laboratory of Polymer Physics and Chemistry, Changchun Institute of Applied Chemistry, Chinese Academy of Sciences, Changchun 130022, P. R. China. E-mail: xiez@ciac.ac.cn*
[c]*University of Science and Technology of China, Hefei 230026, P. R. China*
†Electronic supplementary information (ESI) available. See DOI: 10.1039/c8ob02391c

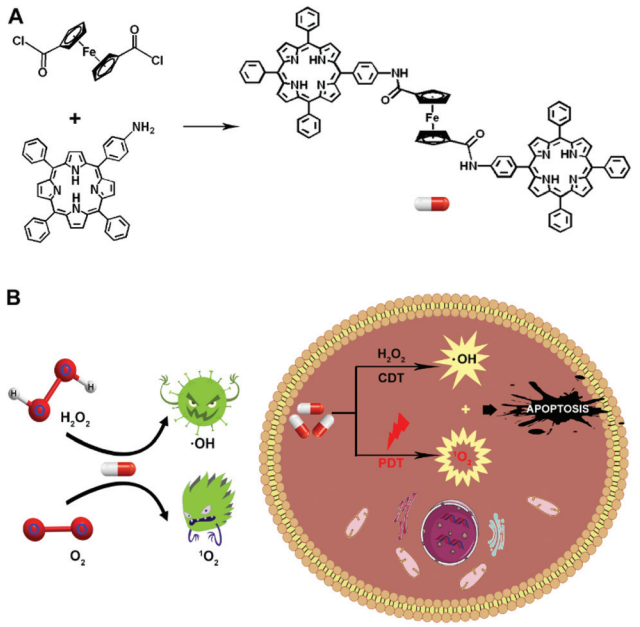

Scheme 1 Schematic illustration of the (A) preparation and (B) application of TNCF for cancer therapy.

dynamic therapy has not been explored yet. As shown in Scheme 1B, according to the Fenton reaction, FC reacted with hydrogen peroxide to produce ·OH, which kills tumor cells efficiently. However, the GSH localized in tumor cells can consume ·OH resulting in the inhibition of CDT. Furthermore, $^1O_2$ produced by the PDT of TPP-NH_2 will decrease the level of GSH, which shows the synergistic therapy efficacy. The obtained TNCF can be well internalized by cells and consume GSH *in vivo*, thereby improving the effectiveness of CDT.

Experimental

Materials and characterization

Milli-Q water was obtained from a Milli-Q system (Millipore, USA). Pyrrole, benzaldehyde, chloroform ($CDCl_3$) and ethanedioylchloride ($(COCl)_2$) were purchased from Sigma-Aldrich Co., Ltd (St Louis, MO, USA). Triethylamine and trifluoroacetic acid (TFA) were purchased from Energy Chemical Co., Ltd. Dulbecco's modified Eagle's medium (DMEM), RPMI-1640 Medium, and fetal bovine serum (FBS) were purchased from Sigma-Aldrich. MTT (3-[4,5-dimethylthiazol-2-yl]-2,5-diphenyltetrazoliumbromide), Lyso-Tracker Green and 4,6-diamidino-2-phenylindole (DAPI) were purchased from Beyotime Biotechnology Co., Ltd (China). A Live–Dead Cell Staining Kit was purchased from KeyGen Biotech Co., Ltd. All of the other chemicals were obtained commercially and used without further purification.

^1H NMR spectra were recorded on an Agilent Mercury 400 MHz spectrometer in chloroform-d. Fluorescence emission spectra were obtained using a Hitachi fluorometer (F-7500 model). The UV-vis spectroscopy study was performed on a Shimadzu UV-vis spectrophotometer (UV-1800 model). Confocal microscopy imaging was performed using a Zeiss LSM 700 confocal microscope and the images were analyzed using ImageJ (NIH). The mass spectra (MS) of the samples were obtained by using a German company Bruker autoflex III smart beam mass spectrometer (MALDI-TOF/TOF).

Synthesis procedures of TPP-NH_2. TPP-NH_2 was synthesized from tetraphenylporphyrin (TPP) in three steps according to the reported methods.

Synthesis procedures of TNCF. Dicarboxyferrocene (FC) reacts with TPP-NH_2 after chlorination to form the target product TNCF. FC (274 mg, 1 mmol) and $(COCl)_2$ (317.5 mg, 2.51 mmol) were added to a round bottom flask. Then, 100 mL of anhydrous tetrahydrofuran and *N*,*N*-dimethylformamide (0.2 mL) were added under argon. The reaction mixture was stirred at room temperature for 24 h. The $(COCl)_2$ was removed by reduced pressure distillation and extracted with $CHCl_3$. TPP-NH_2 (705.1 mg, 1.12 mmol) and dicarboxyferrocene chloride were dissolved in $CHCl_3$ under argon. The reaction was carried out at room temperature for 24 h. Then, the solvent was removed by evaporation, and the crude product was purified by column chromatography on silica.

Singlet oxygen generation measurements

In order to study the ability of TNCF to produce singlet oxygen, DPBF is used as an indicator for detection by using ultraviolet visible spectra. The mixture of DPBF and TNCF is illuminated under a 620 nm lamp at 12 mW cm^{-2}. The absorption value of the DPBF at 415 nm was recorded once every 10 s. The experiment was repeated with a separate DPBF as a control group.

To detect the ability of TNCF to produce hydroxyl radicals (·OH) due to the occurrence of the Fenton reaction, salicylic acid was introduced as a probe. TNCF and salicylic acid were mixed, then hydrogen peroxide (H_2O_2) was added and the absorption value of the mixture at 510 nm was immediately recorded.

Cell culture

Human breast cancer (MCF-7) and human cervical cancer (HeLa) cells were cultured with Dulbecco's modified Eagle's medium (DMEM) in a Petri dish, observing the state of the cells and changing the medium in time to facilitate subsequent experiments. The temperature of the culture chamber was 37 °C, and the concentration of carbon dioxide (CO_2) was 5%.

Cellular uptake

Confocal laser scanning microscopy (CLSM) was used to study the cellular uptake of TNCF by MCF-7 cells. First, the MCF-7 cells were incubated for 24 h in 6-well plates, making sure that the number of cells in each well was greater than 20 000. Then, the DMEM was sucked up before adding a dose of 15 μg mL^{-1} of TNCF to each well. The cells were incubated at 37 °C and 4 °C for 0.5, 4 and 6 h, respectively. After that, the DMEM was removed and the cells were washed three times with PBS. After

that, the cells were soaked in 1 mL of 4% formaldehyde and kept at room temperature for 10 min and then washed twice with PBS again. The nuclei of the cells were stained with 4′,6-diamidino-2-phenylindole (DAPI) for 5 min and washed three times with PBS. The samples were examined by CLSM using a Zeiss LSM 700 system (Zurich, Switzerland).

Intracellular ROS detection

Intracellular ROS detection of PDT. CLSM was used to explore the generation of intracellular ROS. The MCF-7 and HeLa cells were grown in a six-well plate with a cover glass. The cells were incubated for 24 h under 37 °C conditions; then the original medium was replaced with a medium with or without the added medicine. Four hours later, the light group received 20 min of exposure. The cells were washed twice with a medium without FBS; then a medium containing DCFH-DA was added as a probe. The cells were continued to be cultured for 30 min at 37 °C and then observed by CLSM as soon as possible (excitation wavelength, 488 nm; emission band-pass, 500–550 nm).

Intracellular ROS detection of CDT. The MCF-7 and HeLa cells were grown in a six-well plate with a cover glass and incubated for 24 hours under 37 °C conditions. After incubation with 1 mL of DCFH-DA (10 μM in FBS-free DMEM) at 37 °C under 5% CO_2 for 20 min, the culture media were then replaced with media (acidulated DMEM of pH = 6.5) containing the following samples: 200 μM H_2O_2, 20 μg mL^{-1} TNCF and a mixture of 200 μM H_2O_2 and 20 μg mL^{-1} TNCF. The cells were further incubated at 37 °C under 5% CO_2. After 2 h, the cells were washed with PBS three times. The level of intracellular ROS was evaluated by detecting the fluorescence of DCF.

Cytotoxicity assay

DMEM was used to dilute TNCF and H_2O_2 to different concentrations. MCF-7 and HeLa cells were cultured and divided into two groups in 96-well cell-culture plates, and then incubated in a culture medium for 24 h. The medium was replaced with different concentrations of TNCF, and the cells were continued to be cultured for 6 h. The first group of cells remained in the dark, and the second group was irradiated with a laser (620 nm, 12 mW cm^{-2}, 30 min). Then 20 μL of MTT (5 mg mL^{-1}) were added to each hole and the cells were incubated for another 4 h. Finally, the liquid in the hole was sucked up and 150 μL of DMSO were added to each well to dissolve the formazan crystals formed. The baseline corrected absorbance at 590 nm (A(570 nm) − A(630 nm)) was applied to calculate the relative number of viable cells. Finally, the plates were shaken for 3 min, while the absorbance of the formazan was measured at 590 nm (A(570 nm) − A(630 nm)) by using a microplate reader.

Live–dead cell staining assay

The cells were planted in a 96-well plate and incubated for 24 h. After 4 h of incubation with TNCF, TPP-NH_2 and FC, the cells were irradiated using a 620 nm LED lamp (12 mW cm^{-2}, 40 min). Then, the cells were stained with calcein-AM/propidium iodide (PI) for 30 min at room temperature. Finally, the results of cell staining were detected by fluorescence microscopy.

Results and discussion

5-(4-Aminophenyl)-10,15,20-triphenylporphyrin (TPP-NH_2) was synthesized using the method previously reported. As shown in Scheme 1A, 1,1′-ferrocenedicarboxylic acid (FDCA) reacts with TPP-NH_2 after acyl chlorination. After being purified by using a silica gel column, the structures of the obtained products were validated by proton nuclear magnetic resonance (^{1}H NMR) (Fig. S1–S3, ESI†) and matrix-assisted laser desorption/ionization time-of-flight mass spectrometry (MALDI-TOF MS), which demonstrated that TNCF was successfully synthesized.

Then, the optical properties of TNCF were investigated using the absorption and photoluminescence (PL) spectra. As shown in Fig. 1A, the absorption spectra of TNCF in *N*,*N*-dimethylformamide (DMF) did not change before and after the laser irradiation with the maximum absorption at 415 nm, indicating good photostability. According to the PL spectrum (Fig. 1B), TNCF has two distinct peaks at about 650 and 750 nm. As shown in Fig. 1B, TNCF has a strong red fluorescence under 365 nm light irradiation.

To explore the ability of TNCF as a CDT reagent to produce $^{\bullet}$OH, salicylic acid was introduced as an indicator, and its absorbance was monitored (Fig. 2A). As shown in Fig. 2A, the $^{\bullet}$OH produced by the Fenton reaction could react with salicylic acid, and the resulting 3-dihydroxybenzoic acid has absorption at 510 nm. In Fig. 2A and B, with the prolongation of time, the absorbance of 2,3-dihydroxybenzoic acid increased, which showed that more $^{\bullet}$OH were produced with the increase of time. The formation of $^{\bullet}$OH at the cell level was further detected *via* confocal laser scanning microscopy (CLSM) by using 2′,7′-dichlorofluorescein diacetate (DCFH-DA) as a probe. The intracellular $^{\bullet}$OH generation of TNCF was studied in human breast cancer (MCF-7) cells. In Fig. S7,† when the concentration of H_2O_2 was 200 μM, MCF-7 cells still had a high survival rate. As shown in Fig. 2C, the cells treated with TNCF and H_2O_2 emitted obvious green fluorescence. Meanwhile, almost no green fluorescence was found in the

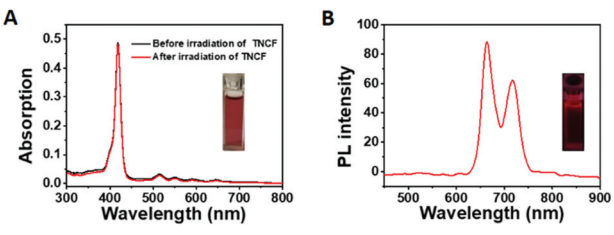

Fig. 1 (A) UV-vis absorption spectra of TNCF (in DMF) with or without laser irradiation; the inset is a picture of TNCF in DMF. (B) PL spectrum of TNCF in DMF; the inset is a photograph of TNCF in DMF upon irradiation with 365 nm light.

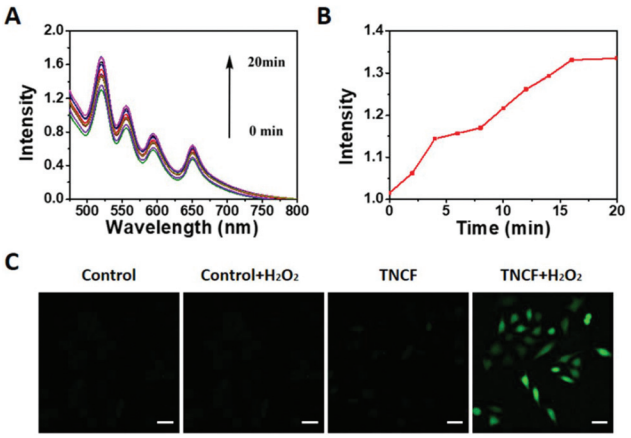

Fig. 2 (A) Time-dependent UV-vis absorption spectra of salicylic acid with H_2O_2 in water (200 μM) from 0 to 20 min. (B) Time-dependent $^{\bullet}OH$ generation kinetics of salicylic acid at 510 nm with H_2O_2 (200 μM). (C) Generation of ROS *in vitro* (MCF-7) denoted by the fluorescence of DCF. Scale bars, 20 μm.

other three control groups. The same results were also observed in human cervical cancer (HeLa) cells (Fig. S8†). These results demonstrated that TNCF could be used as an excellent CDT reagent for tumor therapy.

The ability of TNCF as a PDT reagent to produce ROS under laser irradiation was chemically determined by using 1,3-diphenylisobenzofuran (DPBF) as a pointer, and the absorbance of DPBF was monitored by UV-vis absorption spectroscopy. As shown in Fig. 3A and B, the absorbance of DPBF at 415 nm gradually decreased with increasing illumination time (630 nm, 12 mW cm^{-2}) in the presence of TNCF. In contrast, the absorbance of DPBF with laser irradiation alone was unchanged (Fig. S4B†). The results prove that ROS was produced because of the addition of TNCF. The photostability was investigated by UV-vis absorption spectroscopy. In Fig. S4A,† the absorption peaks of TNCF were basically unchanged under 620 nm laser irradiation (12 mW cm^{-2} for 40 min), indicating its eminent photostability. DCFH-DA was still used as a probe to study the ability of TNCF as a PDT reagent to produce ROS in MCF-7 cells. In Fig. 3C, strong green fluorescence was found in the TNCF + L group (treated with TNCF and laser irradiation) and the TNCF + H_2O_2 + L group (treated with TNCF, H_2O_2 and laser irradiation) compared to the control groups. The same results were found in HeLa cells (Fig. S8†). In short, TNCF has an efficient ability to produce singlet oxygen and can be potentially used as a photosensitive agent for PDT.

The cellular uptake of TNCF by MCF-7 cells was verified by CLSM. The cellular nuclei were stained blue with 4,6-diamidino-2-phenylindole (DAPI). Time dependent internalization of TNCF was observed. As the time extended from 0.5 to 6 h, the intensity of the fluorescence increased (Fig. S5†). When the temperature was reduced from 37 to 4 °C, the fluorescence intensity decreased significantly (Fig. S6†), revealing an ATP-mediated endocytosis pathway. As shown in Fig. 4, after incubation with TNCF for 2 h, the cells were stained with Lyso-Tracker Green and continued to be incubated at 37 °C for 30 min. It was found that the green fluorescence coincided well with the red fluorescence, indicating lysosome-mediated endocytosis of TNCF.

The *in vitro* cytotoxicity of TNCF against MCF-7 cells was evaluated by 3-(4,5-dimethylthiazol-2-yl)-2,5-diphenyltetrazolium bromide (MTT) assays. In order to investigate the CDT effect of TNCF, the cells were treated with or without H_2O_2 for 1 h in advance. We first studied the dark toxicity of TNCF, TPP-NH_2 and FC against MCF-7 cells, and no obvious cytotoxicity was observed in the absence of H_2O_2, denoting their pronounced cytocompatibility without laser irradiation (Fig. 5A). Then the MCF-7 cells were incubated with H_2O_2 for 1 h and subsequently FC, TPP-NH_2 and TNCF were added respectively. TNCF and FC showed conspicuous cytotoxicity toward MCF-7 cells compared with TPP-NH_2 because of CDT (Fig. 5B). We then incubated the cells with TNCF, TPP-NH_2 and FC for 6 h and later irradiated the cells using an LED lamp at a power density of 12 mW cm^{-2} for 40 min. As shown

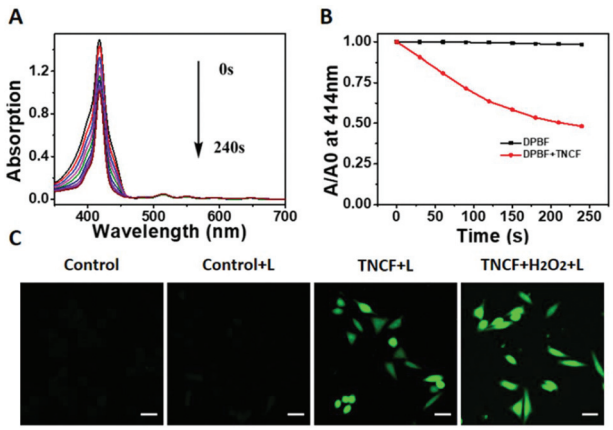

Fig. 3 (A) Time-dependent UV-vis absorption spectra of a mixture of DPBF and TNCF in DMF upon irradiation with a 620 nm laser (12 mW cm^{-2}) from 0 to 240 s. (B) Comparison of the decline rate of DPBF alone and a mixture of DPBF and TNCF under laser irradiation. (C) Generation of ROS *in vitro* under laser irradiation (620 nm, 12 mW cm^{-2}, 40 min) denoted by the fluorescence of DCF. Scale bars, 20 μm.

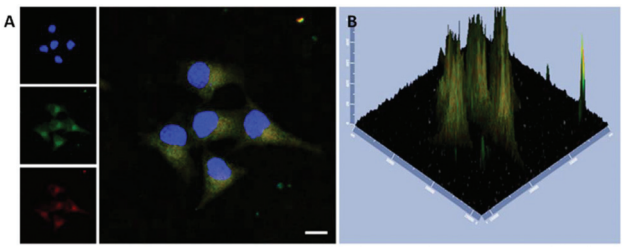

Fig. 4 (A) CLSM images of MCF-7 cells incubated with TNCF in the presence of Lyso-Tracker Green. For each panel, the images show cell nuclei stained with DAPI (blue), the fluorescence of TNCF (red), lysosomes stained with Lyso-Tracker Green (green) and overlays of three images. Scale bars, 20 mm. (B) Fluorescence of TNCF and Lyso-Tracker Red in cells in 2.5D mode.

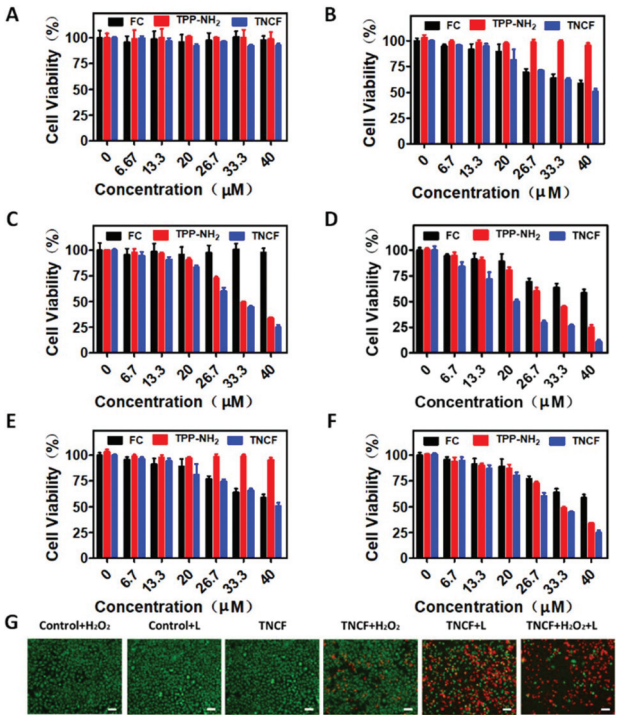

Fig. 5 *In vitro* cytotoxicity of TNCF, TPP-NH_2 and FC against MCF-7 cells: (A) dark and (B) H_2O_2 (0.2 mM). (C) Phototoxicity at different concentrations of porphyrin (0–40 μM) with an LED lamp at a power density of 12 mW cm^{-2} for 40 min and (D) H_2O_2 and an LED lamp. *In vitro* cytotoxicity of TNCF, TPP-NH_2 and FC against MCF-7 cells which have been pretreated with NEM (0.5 mM): with (E) or without (F) an LED lamp. (G) Fluorescence images of calcein-AM (green, live cells) and PI (red, dead cells) co-stained MCF-7 cells after different treatments. Scale bars: 100 μm.

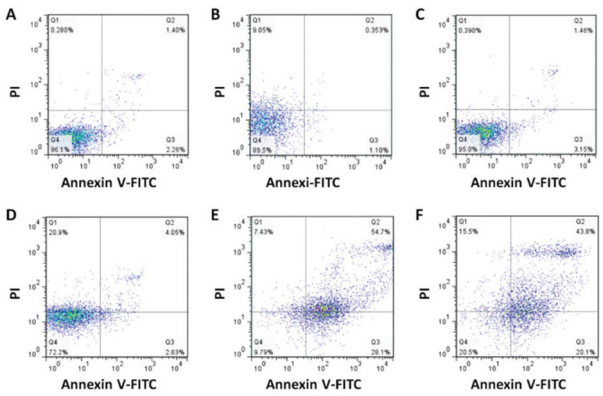

Fig. 6 Flow cytometry analysis of the MCF-7 cells treated with (A) only H_2O_2, (B) only irradiation, (C) only TNCF, (D) TNCF + H_2O_2, (E) TNCF + L, and (F) TNCF + H_2O_2 + L (L = irradiation at 620 nm, 12 mW cm^{-2}, 40 min). The four areas represent different phases of the cells: necrotic (Q1), late-stage apoptotic (Q2), early apoptotic (Q3), and live (Q4).

in Fig. 5C, TNCF and TPP-NH_2 showed a dramatic photocytotoxicity toward MCF-7 cells compared with FC. The IC_{50} values of the three kinds of agents were 25 μM, 29.7 μM and >50 μM, respectively. These results substantiated the superiority of TNCF as a potential PDT agent. Interestingly, the IC_{50} value of TNCF is less than TPP-NH_2, and we boldly assume that there is synergy between PDT and CDT. GSH can consume $^{\bullet}OH$ *in vivo*, which reduces the cytotoxicity of CDT. We introduced *N*-ethylmaleimide (NEM) to reduce the GSH content in the cells in order to enhance the efficacy of FC.[49–54] We first incubated the cells for 1 h with NEM and then added FC, TPP-NH_2 and TNCF, respectively. Fig. 5E shows a very similar result to that of H_2O_2 treatment.

To observe the therapeutic effect intuitively, the cells were differentiated by live/dead cell staining. Live cells displayed green color after being stained with calcein-AM, and dead cells displayed red color when dyed with propidium iodide (PI). In Fig. 5G, almost no red fluorescence appeared in the three control groups. The cells treated with TNCF and H_2O_2 have some red fluorescence because of the result of CDT. A large amount of red fluorescence appears in the cells after being treated with TNCF and laser irradiation, which result from PDT. For the cells treated with TNCF, H_2O_2 and irradiation, almost no living cell was seen, validating the efficacy of dual CDT and PDT. These results were in accordance with that of MTT.

To explore the anti-cancer mechanism, the MCF-7 cells with various treatments were stained with fluorescein isothiocyanate (V-FITC) and PI for the flow cytometry analysis. Compared with the control groups, the mortality rates (Q2 + Q3) are 1.45% and 3.66% for the cells treated with laser irradiation and H_2O_2, respectively, as compared to 90.5% of mortality for those treated with both laser irradiation and H_2O_2. These results were consistent with the MTT assays, which showed that TNCF possesses the effect of CDT and PDT (Fig. 6).

Conclusions

In conclusion, we have designed and synthesized an agent by the reaction of a photosensitizer TPP-NH_2 and a chemical anticancer drug FC, which was applied in CDT and PDT. As an effective photosensitizer, TNCF can transform O_2 into $^{\bullet}O_2^-$ under the irradiation of an LED lamp for PDT. What's more, the Fenton or Fenton-like reaction can significantly improve the cytotoxicity under irradiation. TNCF can consume glutathione and overcome tumor hypoxia by catalyzing H_2O_2 to produce O_2. TNCF can achieve a synergistic effect between CDT and PDT, and lead to enhanced cytotoxicity, which possesses great potential in cancer treatment.

Conflicts of interest

There are no conflicts to declare.

Acknowledgements

Financial support was kindly provided by the National Science Foundation of China (Project No. 51522307).

Notes and references

1 S. L. Fenn, T. Miao, R. M. Scherrer and R. A. Oldinski, *ACS Appl. Mater. Interfaces*, 2016, **8**, 17775–17783.
2 J. S. Arora, H. Y. Murad, S. Ashe, G. Halliburton, H. Yu, J. He, V. T. John and D. B. Khismatullin, *Mol. Pharmaceutics*, 2016, **13**, 3080–3090.
3 N. Bhattarai, M. Chen, R. L. Pérez, S. Ravula, P. Chhotaray, S. Hamdan, K. McDonough, S. Tiwari and I. M. Warner, *J. Mater. Chem. B*, 2018, **6**, 5451–5459.
4 X. Feng, Y. Shi, L. Xie, K. Zhang, X. Wang, Q. Liu and P. Wang, *J. Med. Chem.*, 2018, **61**, 7189–7201.
5 J. Yan, W. He, S. Yan, F. Niu, T. Liu, B. Ma, Y. Shao, Y. Yan, G. Yang and W. Lu, *ACS Nano*, 2018, **12**, 2017–2026.
6 H. Abrahamse and M. R. Hamblin, New photosensitizers for photodynamic therapy, *Biochem. J.*, 2016, **473**(4), 347–364.
7 Y. Dai, Z. Yang, S. Cheng, Z. Wang, R. Zhang, G. Zhu, Z. Wang, B. C. Yung, R. Tian and O. Jacobson, *Adv. Mater.*, 2018, **30**, 1704877.
8 K. T. Lee, Y. J. Lu, F. L. Mi, T. Burnouf, Y. T. Wei, S. C. Chiu, E. Y. Chuang and S. Y. Lu, *ACS Appl. Mater. Interfaces*, 2017, **9**, 1273–1279.
9 Y. Liu, W. Zhen, L. Jin, S. Zhang, G. Sun, T. Zhang, X. Xu, S. Song, Y. Wang, J. Liu and H. Zhang, *ACS Nano*, 2018, **12**, 4886–4893.
10 L. S. Lin, J. Song, L. Song, K. Ke, Y. Liu, Z. Zhou, Z. Shen, J. Li, Z. Yang and W. Tang, *Angew. Chem., Int. Ed.*, 2018, **57**, 4902.
11 H. Lin, Y. Chen and J. Shi, *Chem. Soc. Rev.*, 2018, **47**, 1938–1958.
12 L.-Y. Duan, Y.-J. Wang, J.-W. Liu, Y.-M. Wang, N. Li and J.-H. Jiang, *Chem. Commun.*, 2018, **54**, 8214–8217.
13 S. Callaghan, M. A. Filatov, E. Sitte, H. Savoie, R. W. Boyle, K. J. Flanagan and M. O. Senge, *Photochem. Photobiol. Sci.*, 2017, **16**, 1371–1374.
14 C. Zhu, D. Huo, Q. Chen, J. Xue, S. Shen and Y. Xia, *Adv. Mater.*, 2017, **29**, 1703702.
15 C. Zhang, W. Bu, D. Ni, S. Zhang, Q. Li, Z. Yao, J. Zhang, H. Yao, Z. Wang and J. Shi, *Angew. Chem., Int. Ed.*, 2016, **128**, 2141–2146.
16 M. X. Wu and Y. W. Yang, *Adv. Mater.*, 2017, **29**, 1606134.
17 X. Chen, F. Wang, J. Y. Hyun, T. Wei, J. Qiang, X. Ren, I. Shin and J. Yoon, *Chem. Soc. Rev.*, 2016, **45**, 2976–3016.
18 Y. Wang, W. Yin, W. Ke, W. Chen, C. He and Z. Ge, *Biomacromolecules*, 2018, **19**, 1990–1998.
19 C. Liu, W. Chen, Z. Qing, J. Zheng, Y. Xiao, S. Yang, L. Wang, Y. Li and R. Yang, *Anal. Chem.*, 2016, **88**, 3998–4003.
20 W.-P. Li, C.-H. Su, Y.-C. Chang, Y.-J. Lin and C.-S. Yeh, *ACS Nano*, 2016, **10**, 2017–2027.
21 F. Muhammad, W. Qi, A. Wang, J. Gu, J. Du and G. Zhu, *J. Mater. Chem. B*, 2015, **3**, 1597–1604.
22 Y. Li, X. Zheng, X. Zhang, S. Liu, Q. Pei, M. Zheng and Z. Xie, *Adv. Healthcare Mater.*, 2016, **6**, 1600924.
23 H. Abrahamse and M. R. Hamblin, *Biochem. J.*, 2016, **473**, 347–364.
24 X. Zheng, Z. Li, L. Chen, Z. Xie and X. Jing, *Chem. – Asian J.*, 2016, **11**, 1780–1784.
25 W. Zhang, W. Lin, X. Zheng, S. He and Z. Xie, *Chem. Mater.*, 2017, **29**, 1856–1863.
26 X. Zheng, L. Wang, Q. Pei, S. He, S. Liu and Z. Xie, *Chem. Mater.*, 2017, **29**, 2374–2381.
27 X. Zheng, L. Wang, S. Liu, W. Zhang, F. Liu and Z. Xie, *Adv. Funct. Mater.*, 2018, **28**, 1706507.
28 K. Chang, Y. Tang, X. Fang, S. Yin, H. Xu and C. Wu, *Biomacromolecules*, 2016, **17**, 2128–2136.
29 P. Liang, Q. Tang, Y. Cai, G. Liu, W. Si, J. Shao, W. Huang, Q. Zhang and X. Dong, *Chem. Sci.*, 2017, **8**, 7457–7463.
30 B. Breiner, K. Kaya, S. Roy, W. Y. Yang and I. V. Alabugin, *Org. Biomol. Chem.*, 2012, **10**, 3974–3987.
31 P. Bhattacharya, A. Basak, A. Campbell and I. V. Alabugin, *Mol. Pharmaceutics*, 2018, **15**, 768–797.
32 X. Zheng, L. Wang, M. Liu, P. Lei, F. Liu and Z. Xie, *Chem. Mater.*, 2018, **30**, 6867–6876.
33 M. Mohankumar, M. Holler, E. Meichsner, J.-F. Nierengarten, F. Niess, J.-P. Sauvage, B. Delavaux-Nicot, E. Leoni, F. Monti, J. M. Malicka, M. Cocchi, E. Bandini and N. Armaroli, *J. Am. Chem. Soc.*, 2018, **140**, 2336–2347.
34 Q. Zou, M. Abbas, L. Zhao, S. Li, G. Shen and X. Yan, *J. Am. Chem. Soc.*, 2017, **139**, 1921–1927.
35 K. Liu, R. R. Xing, Y. X. Li, Q. L. Zou, H. Möhwald and X. H. Yan, *Angew. Chem., Int. Ed.*, 2016, **55**, 12503–12507.
36 C. S. Jin, J. F. Lovell, J. Chen and G. Zheng, *ACS Nano*, 2013, **7**, 2541–2550.
37 J. Wang, Y. Zhong, X. Wang, W. Yang, F. Bai, B. Zhang, L. Alarid, K. Bian and H. Fan, *Nano Lett.*, 2017, **17**, 6916–6921.
38 Y. Zhou, X. Liang and Z. Dai, *Nanoscale*, 2016, **8**, 12394–12405.
39 D. Wang, L. Niu, Z.-Y. Qiao, D.-B. Cheng, J. Wang, Y. Zhong, F. Bai, H. Wang and H. Fan, *ACS Nano*, 2018, **12**, 3796–3803.
40 Y. Cao, H. Dong, Z. Yang, X. Zhong, Y. Chen, W. Dai and X. Zhang, *ACS Appl. Mater. Interfaces*, 2017, **9**, 159–166.
41 F. Bolze, S. Jenni, A. Sour and V. Heitz, *Chem. Commun.*, 2017, **53**, 12857–12877.
42 Q. Yu, Y. Han, X. Wang, Q. Chen, Z. Dong, Z. Yi, C. Jiang, X. Yin and C. Wu, *ACS Nano*, 2018, **12**, 2695–2707.
43 J. Chen, S. Lei, K. Zeng, M. Wang, A. Asif and X. Ge, *Nano Res.*, 2017, **10**, 2351–2363.
44 Y. Zhou, F. Huang, Y. Yang, P. Wang, Z. Zhang, Y. Tang, Y. Shen and K. Wang, *Small*, 2018, **14**, 1702446.
45 R. X. Zhang, L. Y. Li, J. Li, Z. Xu, A. Z. Abbasi, L. Lin, M. A. Amini, W. Y. Weng, Y. Sun, A. M. Rauth and X. Y. Wu, *Adv. Funct. Mater.*, 2017, **27**, 1700804.
46 X. Xu, P. E. Saw, W. Tao, Y. Li, X. Ji, S. Bhasin, Y. Liu, D. Ayyash, J. Rasmussen and M. Huo, *Adv. Mater.*, 2017, **29**, 1700141.
47 A. N. Cammidge, P. J. Scaife, G. Berber and D. L. Hughes, *Org. Lett.*, 2005, **7**, 3413–3416.

48 V. S. Shetti and R. Mangalampalli, *Eur. J. Org. Chem.*, 2010, 494–508.
49 L. Hu and R. F. Colman, *Biochemistry*, 1997, **36**, 1635–1645.
50 G.-J. Kim, K. Lee, H. Kwon and H.-J. Kim, *Org. Lett.*, 2011, **13**, 2799–2801.
51 R. Svensson, J. Alander, R. N. Armstrong and R. Morgenstern, *Biochemistry*, 2004, **43**, 8869–8877.
52 W. Zhang, W. Lin, Q. Pei, X. Hu, Z. Xie and X. Jing, *Chem. Mater.*, 2016, **28**, 4440–4446.
53 J. Ding, F. Shi, C. Xiao, L. Lin, L. Chen, C. He, X. Zhuang and X. Chen, *Polym. Chem.*, 2011, **2**, 2857–2864.
54 M. H. Lee, J. H. Han, P.-S. Kwon, S. Bhuniya, J. Y. Kim, J. L. Sessler, C. Kang and J. S. Kim, *J. Am. Chem. Soc.*, 2012, **134**, 1316–1322.